Addendum to Proceedings of SCANNING 2000
May 9–12, 2000
San Antonio, Texas, USA

Electron Microscopy of Squamous Cell Carcinoma of the Head and Neck

MARIA ALBERTSSON

Dept. of Oncology, University Hospital, Lund, Sweden

Squamous cell carcinoma of the head and neck carries a bad prognosis. The most important thing to attain in order to achieve cure is local tumor control. The main therapy available is external radiotherapy, which can be supplemented when necessary with interstitial radiotherapy, chemotherapy and surgery. In this paper we have evaluated specimens from thirty-five patients with squamous cell carcinoma of the head and neck. The specimens were taken before therapy in the process of staging. Scanning electron microscopy (SEM) and transmission electron microscopy (TEM) analyses were made. On SEM, the parameters analyzed were the amount and appearance of microvilli, filaments and blood vessels. On TEM scoring was made of the filaments, desmosomes, nuclei, nucleoli, mitochondria and blood vessels.

Scoring of the samples showed a difference between the group with recurrent disease (N=10, group A) and the group with local tumor control (N=25, group B) regarding blood vessels and intracellular filaments.

Multi-photon Excited Fluorescence Spectra of Common Bio-probes

PING-CHIN CHENG, FU-JEN KAO*, CHI-KUANG SUN†, BAI-LING LIN‡, TZU-MING LIU†, YUNG-SHENG WANG*, MAO-KUO HUANG*, YI-MIN WANG*, JIAN-CHENG CHEN*, I. JOHNSON¶

AMIL, Department of Electrical Engineering, University at Buffalo, Buffalo, NY, USA; *Department of Physics, National Sun Yat-sen University, Kaohsiung, Taiwan, Republic of China; †Department of Electrical Engineering, National Taiwan University, Taipei, Taiwan, Republic of China; ‡Institute of Molecular Biology, Academia Sinica, Taipei, Taiwan, Republic of China; ¶Molecular Probes Inc., Eugene, OR, USA

Fluorescent probes are commonly used in biological fluorescence microscopy for tracking specific structures and subcellular compartments, and for indicating cellular ionic conditions. Recent development in multi-photon fluorescence microscopy has greatly expanded the usage of fluorescent probes in biomedical research. Considering its non-linear nature, two-photon excitation may generate very different fluorescence spectral response in the sample when compared with single photon excitation[1,3,4]. It is thus necessary to measure the two-photon spectra of various fluorescent probes, so that two-photon fluorescence microscopy may be performed effectively and the images properly interpreted. This report represents the second installment of a continued effort in characterizing the multi-photon fluorescence spectra of commonly used bio-probes[2].

Two-photon fluorescence spectra excited with near infrared at 780nm were obtained with a SpectraPro-500 spectrophotometer (Acton Research) equipped with a TE-cooled PMT and coupled to a Spectra-Physics Tsunami Ti-sapphire laser pumped by a Coherent Verdi solid-state laser operated at 85MHz, 100fs pulse. The 1240nm infrared (IR) excitation was obtained from a Spectra-Physics Millianin IR (1064nm) pumped Chromium-doped Forsterite laser (built by CKS) operated at 120MHz, 130fs pulse. A cooled CCD array spectrophotometer (Acton Research) was used for spectral detection. An Olympus BX microscope trinocular head and an epi-fluorescence beam-splitter housing were modified for the measurements. A 740nm dichroic beam splitter was used for separating the excitation beam and the fluorescence emission. In addition, two IR cut-off filters (Edmond Scientific, Cat. K53-710) were installed in front of the entrance slit of the monochromator to reject scattered IR from the sample. A 4x microscope objective was used to focus the pump beam into a 0.3ml microfuge tube. Two-photon fluorescence images were taken with an Olympus water immersion objective (UPLANApo 60x W-PSF, NA=1.2) on an Olympus Fluoview inverted confocal microscope. The same Ti-sapphire laser described above was used for microscopy. A 740nm short-pass dichroic beam splitter was installed in the excitation path of the confocal scanning unit.

Figures 1(a-f) show two-photon pumped fluorescence spectra of six commonly used bio-probes. Measurements of DAPI (Fig. 1a), Hoechst 33258 (Fig. 1b) and Syto 17 [Fig. 1c (Ex=780nm) and Fig. 1d (Ex=1240nm)] were performed with 2μM dye in the presence of 160μg/ml fragmented salmon sperm DNA in TE buffer (10mM Tris, 1mM EDTA, pH7.4). This concentration approximates 50 base pairs of DNA per dye molecule. Methanol solutions of MitoTracker® (Molecular Probe M-7512; Fig. 1e) and LysoTracker Red®(Molecular Probe L-7528; Fig. 1f) were used in the measurement. Spectra e and f were excited with IR at 1240nm, therefore; the MitoTracker® emission is the result of three-photon excitation, while the spectrum of

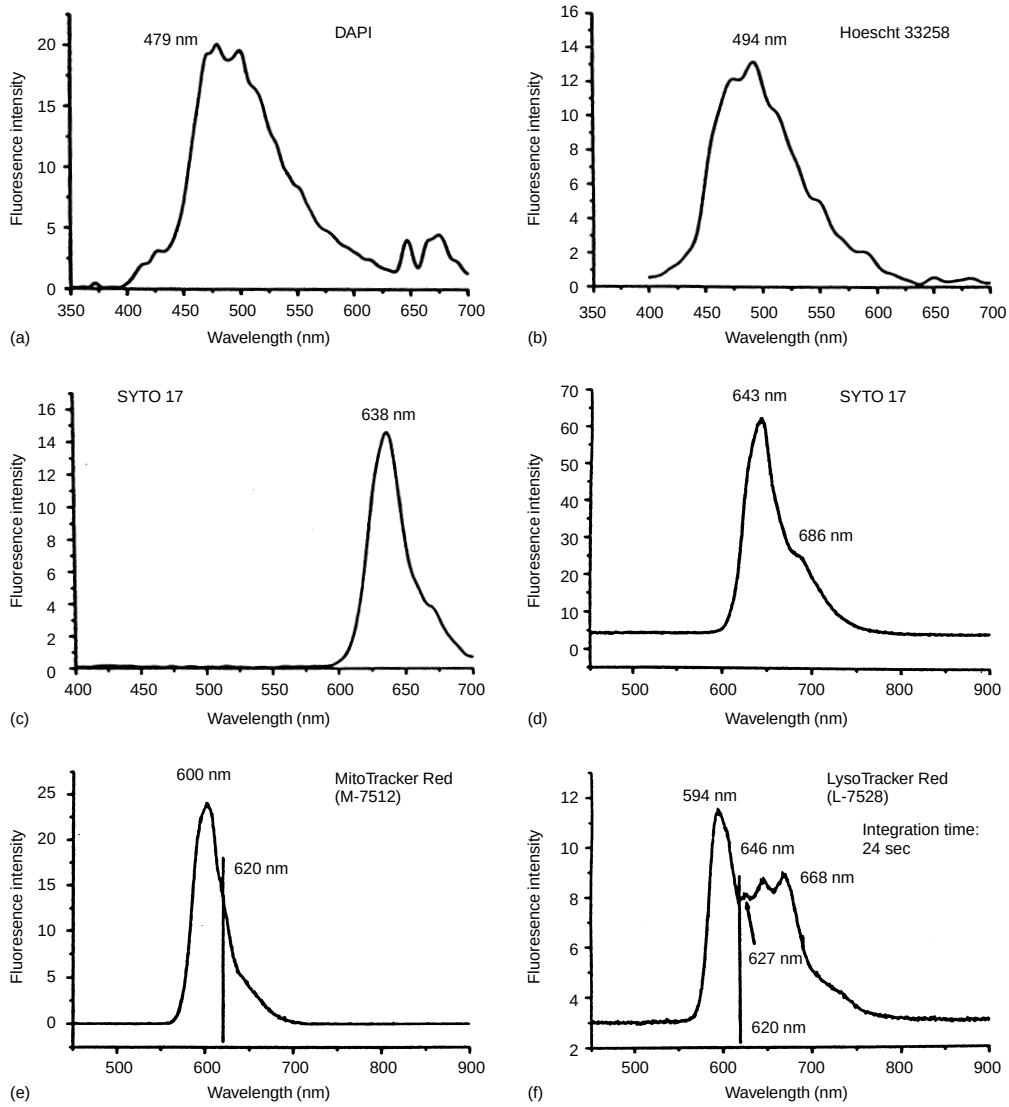

FIG. 1 Two-photon pumped fluorescence spectra of DAPI (a) (Ex=780nm), Hoechst 33258 (b) (Ex=780nm), SYTO 17 (c) (Ex=780nm) and (d) (Ex=1240nm), Mitotracker® (e) (Ex=1240nm), and Lysotracker® (f) (Ex=1240nm).

LysoTracker® is a mixed result of two and three-photon excitation.

This project was support by Academia Sinica (BLL), the National Science Council [NSC-88-2811-B-001-0023(PCC), NSC-89-2311-B-001-032(BLL), NSC89-2112-M-110-016(JFK), NSC89-2216-E-110-003(FJK), NSC89-2215-E-002-004 (CKS)], Academic Excellence Program of the Ministry of Education (89-B-FA08-1-4), Republic of China and Mr. and Mrs. Jin-Mu Huang of Aurum Belle Investment Co (on behalf of the Ge-An Charity) to PCC. Fluorescent probes were provided by Molecular Probes, Inc. Eugene, OR, USA. PCC, FJK, CKS and BLL contribute equally, therefore should be considered as co-principal authors.

References

1. Cheng, PC, Pan SJ, Shih A, Kim KS, Liou WS and Park MS: Highly efficient upconverters for multiphoton fluorescence microscopy. *J. Microscopy* 189:199-212,1997
2. Cheng PC, Lin BL, Kao FJ, Sun CK and Johnson I.: Multi-photon Excited Fluorescence Spectrum of Common Nucleic Acid probes, *Microsc Microanal*, 6, Proceedings issue, in press, 2000
3. Kao FJ, Lin BL and Cheng PC: Multi-photon fluorescence micro-spectroscopy, *SPIE Proceedings*, 3919, in press, 2000
4. Kao FJ, Lin BL and Cheng PC: Multi-photon fluorescence micro-spectroscopy of plant tissues, *Microsc Microanal*, 6, Proceedings issue, in press, 2000

The Study of Vascular Development in the Stem of *Na1* Mutant in Maize by Confocal Microscopy

WAYNE Y. CHENG, PING-CHIN CHENG* AND DAVID B. WALDEN†

Williamsville East High School, Williamsville, NY, USA; *Advanced Microscopy and Imaging Laboratory, Department of Electrical Engineering, State University of New York, Buffalo, NY, USA; †Department of Plant Sciences, University of Western Ontario, London, Ontario, Canada

Laser scanning confocal microscopy has made three-dimensional study of biological structure feasible. Although high numerical aperture objective lenses are commonly used to achieve high spatial resolution, confocal microscopy at low magnification can be useful in the study of vascular arrangement in plants. We report here some preliminary observations on the vasculature and node development of a dwarf mutant (*na1*) in maize. The homozygous nana-1 plant (*na1/na1*) is characterized as short erect dwarf (Hutchison, 1922; Li, 1933)(Fig. 1a); different from some other dwarf mutants, the phenotype does not respond to treatment of gibberellins. The recessive *na1* allele is located on the long arm of chromosome 3 (3L-113).

Maize (*Zea mays* L., var. Ohio 43 and *na1* mutant) plants were grown in 1998 and 1999 summer nursery at the field-station of University of Western Ontario, London Ontario, Canada. Plants at approximately 2 months old were fixed in 1:3 acetic acid/ EtOH. Multiple changes of fixative were made for a period of a month to remove as much pigmentation as possible. The specimen was then washed thoroughly, stained in diluted Schiff's reagent (10%), washed in 0.1M metabisulphate solution (with 1 ml of 1 N HCl per liter), dehydrated in EtOH and cleared in methyl salicylate (Cheng *et al.*, 1995). A series of optical slices was obtained from 3-5mm thick sections of the stem by using an Olympus Fluoview confocal microscope with a 4x objective lens. The 514nm emission line of an Ar ion laser was used as the illumination source, and fluorescence emission longer than 590nm was detected.

The dwarf character of *na1* homozygous is associated with an abnormal development in the stem (Cheng *et al.*, 2000a, b). Instead of the well-defined nodes and internodes found in the wild type (+/+) stem, *na1/na1* develops a stem lacking organized nodal and internodal vasculature. Different from the parallel-arranged longitudinal vascular bundles, commonly found in the internodes of heterozygous and wild type plants, *na1* homozygous develops poorly organized vascular bundles. In addition, the interconnecting vascular bundles are not limited to the nodal region as found in the wild type, but can be found at any level of the stem (Fig. 1b, x). The lack of a well-defined node structure is clearly evident. In wild type, the leaf vascular bundles originate from nodes, in contrary, the leaf vascular bundles of *na1/na1* do not initiate from a definable

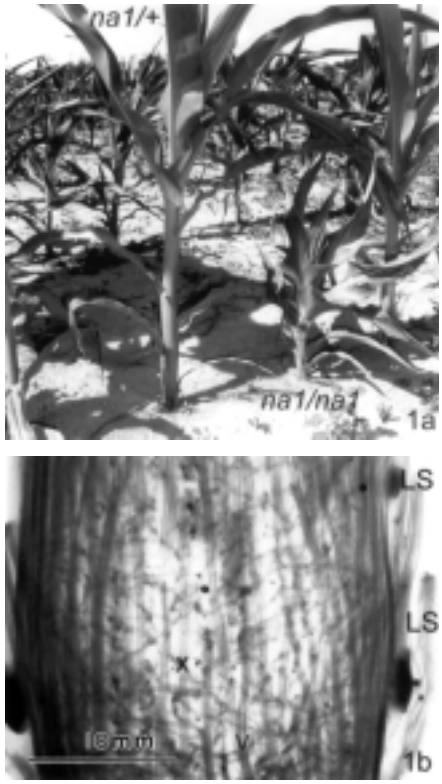

FIG. 1 (a) The picture shows field grown heterozygous (*na1*/+) and homozygous *(na1/na1)* plants. These plants were approximately 60 days old. (b) Longitudinal section of a *na1/na1* plant showing the organization of vascular bundles (V) in stem and the insertion of leaves (LS)

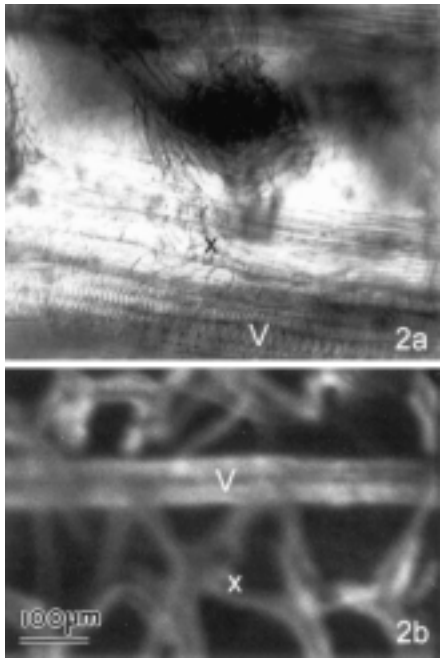

FIG. 2 (a) Longitudinal section of a na1/na1 plant showing the branching of interconnecting members (x) from the vascular bundle (V). (b) Extended focus image of a *na1/na1* stem showing the major vascular bundle (V) and the irregular interconnecting members (x).

node. In addition, numerous interconnecting vasculatures (Fig. 2a, x) can be visualized at every level of the stem.

Under laser scanning confocal microscopy, a complex three-dimensional vascular network is evident. Fig. 2b show extended-focus image of the vasculature in *na1/na1* stem. In addition to the large vascular bundle (V) running generally along the axis of the stem, there are numerous small xylem elements (x) interconnected to form a complex mash.

References

C. B. Hutchison (1922): Cornell Univ. Exp. Syn. Momoir. 60. 1419–1473

H. W. Li (1933), J. Hered. 24. 279–281

P. C. Cheng (1995): Method for studying vascular bundle in 3D, *Maize Genetic Cooperation Newsletter*, 69, 28

W. Y. Cheng et al. (2000): Abnormal node development in *na1/na1*, Maize Genetic Cooperation Newsletter, 74. (in press)

W. Y. Cheng, P. C. Cheng and D. B. Walden (2000): Abnormal vasculature in the stem of *nana-1* mutant in maize — a confocal microscopy study, *Microsc Microanal.*, 6 Proceedings issue (in press)

Processing GSR (Gun Shot Residue) Samples by SEM/EDX Technique — Advantages & Disadvantages

PETER FLENER

Dept. of Forensic Science & Research, Federal Ministry of the Interior, Vienna, Austria

The detection and identification of gun shot residue (GSR) samples by scanning electron microscopy (SEM) coupled with energy dispersive x-ray spectrometry (EDX) is well established and frequently used by most of the recent equipped forensic institutes and crime laboratories worldwide.

The reason seems to be quite simple: The sampling technique is very easy to learn and to put into practice. Taking samples from suspects in Austria is mainly done by police officers.

The analysis of the samples is performed by a "fully automated computer controlled analyzing system called SEM/EDX which generates a self-explanatory expertise for the court."

A lot of people in my surroundings are thinking that way; in my opinion – that's fiction.

In Austria there are instructions existing as to how to take microparticle-samples from a person or a dead body. At first the examiner has to watch and describe what he is seeing on the hands; e.g., (visible) dirt, blood strains, etc. After that, he has to take the samples using the "sticky lift technique".

Zeichner[1] mentioned in his paper that the "overall" success rate on the examined samples is about 10% (1995 at the Israel Police HQ, Forensic Science Laboratory). Five years later it seems that the "overall success rate" did not increase dramatically. In addition to the well known complications such as "to keep the time elapsed between firing and sampling short", "the threshold setting of the backscatter detector for automated GSR particle search", "the influence of dirt and crusts of dried blood on the hands before sampling", some further disadvantages occurred. These are summarized under the topic "contamination". We did have the experience that under the influence of the electric field in the column of an SEM, charged GSR and other particles are able to "jump" from one aluminum stub coated with conducting sticky tape to another. Examining stubs from different cases mounted on the same specimen holder in the same batch (SEM/EDX run) could provide serious problems. Contamination brought in from the examiner (technician) should be avoided; using "clean room technique" will be the best choice if money is not really the problem. Another fact which should be mentioned, is presence of look-a-like GSR particles, such as remains from fireworks or sparklers.

Nowadays, processing GSR samples by SEM/EDX technique seems to be the best method to handle the problem: did a person fire a gun, or not. No other method allows us to identify GSR particles in itself. Bulk techniques like FAAS provide fractions of the concentration of the elements lead, barium and antimony, which are typical for GSR, but there is no further information about the original particles available, because the substrate is dissolved.

The interpretation of GSR results can cause a lot of problems if there are only one, two or three GSR particles on a stub. Is it possible to distinguish whether a person fired a gun or only touched a gun. However, it cannot be excluded that that small number of GSR particles is the result of contamination.

Finally, what conclusion can we draw? We have to spend a lot of time to check the results very carefully. Taking blank samples could also be very useful.

In my opinion, it does not make very much sense ending an expertise with the result: 2 GSR particles could be observed – nothing more. Using the best expertise possible, you have to link your result from the REM/EDX analysis to the other facts of the crime case to provide an interpretation which will be helpful in court.

References

1. Zeichner A, Levin N: Casework Experience of GSR Detection in Israel, on Samples from Hands, Hair and Clothing Using an Autosearch SEM/EDX System. JFSCA, Vol.40, No.6, 1082-1085 (1995)

The Molecular Taste of Milk and its Structural Renovation Using Biotechnology

N. C. GANGULI

Former Professor of Medicine, Malviya Nagar, New Delhi, India

Milk is an outstanding fluid with unique chemistry. From time immemorial, milk molecules have been a highly inventive curiosity. Milk has a long-standing reputation as a guaranteed package of balanced nutrients. With the recognition of its food value, milk has attracted a wide spectrum of scientists using it either as a physical, chemical, biological or biotechnological "substrate". They have successfully identified new molecules strengthening the molecular infrastructure. Recently, biotechnologists have taken keen interest in assigning additional bioresponsibilities to the mammary apparatus, either for synthesis or for secretion of new molecules.

Revelation of the molecular mosaic in milk and its biosynthesis during lactation by a variety of mammalian species, has attracted physical chemists to study milk as a unique celloidal system, chemists to delve in search of new chemical molecules, biochemists debating for its precursors and synthesis, technologists attempting to restructure for product manufacture, and the biotechnologists desperately trying to compel the mammary gland to synthesize or secrete value-added molecules in milk. Even in our Ayurvadic language, the Pandits do not lag behind. They tell us that in milk resides molecules with therapeutic value, containing the essence, the RASA, of may medicinal plants. Milk out of a copper vessel calms VATA, out of gold vessel calms PITTA, out of a silver bowl calms XAPHA and from a brass vessel helps to make blood.

In recent times, the application of biotechnology in the field of dairying at large is gaining continuous momentum. It is encompassing a wide spectrum of scientists who have exhibited outstanding contributions in myriad areas of dairying starting from animal breeding, reproduction, feeding, lactation, gene cloning, embryo transfer, and milk with new molecules serving as biopharmacy, designer milk, and low lactose milk by cloning s-glactosidase enzyme. Another group of scientists engaged in new milk products development, are working on formulations contributing monumental products such as humanized milk, bioactive molecules, probiotic milk products, and exploiting the microorganisms by profitable managements.

Using the new knowledge of biotechnology, the future of the dairy industry in India is promising. At the same time, there is a need to develop a strong linkage with the food industry which may yield more assured results in new product development. Keeping in view the above options, there are several new and promising areas in both production and processing of milk as suggested below:

Combinatorial chemistry; designer milk; value added products; new molecules through directed evolution; neosugars production (fructo-oligosaccharides); freeze-dried sperm technology; intracytoplasmic sperm injection technique; sperm sexing; probiotic foods; specific enzyme cloning; nano-scale technology; single molecule behavior in different molecular crowds.

Expression of Neuronal Nicotinic Acetylcholine Receptor α3 and α7 Subunits in Mouse and Compensatory Mechanism in Heterozygous α3 Animals

NABARUN GHOSH, RAMIRO SALAS, LAURA Y. MACKEY*, WEI YU, RON S. BROIDE AND MARIELLA DEBIASI

Division of Neuroscience, *Department of Molecular Physiology and Biophysics, Baylor College of Medicine, Houston, TX, USA

Nicotinic acetylcholine receptors (nAChRs) form a family of pentameric ligand-gated ion channels whose opening is controlled by acetylcholine (ACh) and nAChR agonists. They are key molecules in cholinergic nicotinic transmission at the neuromuscular junction, autonomic ganglia, and in several brain areas (Clementi *et al.*, 2000). Eleven genes have been identified that encode neuronal nAChR subunit: eight α subunits (α2-α9) and three β subunits (β2–β4). The α3 nAChR subunit is highly expressed in the autonomic ganglia and α3-deficient mice manifest multiorgan autonomic dysfunction (Xu *et al.*, 1999). Our data show that the absence of α3 alters NGF content, cell size, cell distribution, and neurotransmitter profile of sympathetic neurons from the superior cervical ganglion. Overall these data suggest that α3 containing nAChRs participate in the development of sympathetic ganglia, and have a dominant role in the autonomic control of peripheral organs. Because little is known about the developmental change in neuronal nAChRs subunit expression (Zoli *et al.*, 1995), we have used *in situ* hybridization techniques with ^{35}S-labeled radioactive riboprobes to study the expression patterns of α3 during development. We examined the pattern and the level of expression of α3 mRNA in the whole bodies of wild type animals at postnatal day 0. In addition we have studied the superior cervical ganglion and the adrenal medulla of mice at postnatal days 10-12.

Observation and Results: Following development of the photographic emulsion and counter-staining, we examined all the tissue sections under bright-field and dark-field microscopy. A qualitative classification of the hybridization signals based on the overall brightness and local accumulation of grains was done by eye. A quantitative classification of the level of hybridization was done by counting the number of silver grain per sq. mm as described by Berman *et al.* (1990). At P0, high levels of α3 expression were recorded in the adrenal medulla, dorsal root ganglia, superior cervical ganglia, spinal cord and different parts of the brain. In the SCG the stronger autoradiography signals were obtained with α3 riboprobes. To determine whether

different functional groups of cells within the same ganglion express different combinations of nAChR subunits we studied the distribution of another nAChR subunit, the α7 subunit. The signal for α7 was distributed on groups of neurons that could be visible as patches under dark-field microscopy.

We found remarkable differences in α7 mRNA expression between α3 +/+ and α3 +/- mice. The α7 mRNA expression was higher in the SCG of α3+/- animals than in that of α3 +/+ animals suggesting the presence of compensatory mechanism in the +/- mice. In the adrenals, the α7 mRNA was found in clusters of cells and seemed to be strongly upregulated in the α3 +/- animals. However, α7 mRNA levels in α3 +/+ and α3 -/- animals were similar with a mild increase in the latter animals, suggesting that the compensatory upregulation of α7 does not occur when α3 is absent.

References

Berman SA, Bursztajn S, Bowen B and Gilbert W. Localization of an acetylcholine receptor intron to the nuclear membrane. *Science*. 1990; 247:212-214

Clementi F, Fornasari D, and Gotti C. Neuronal nicotinic acetylcholine receptors: from structure to therapeutics. *Trends in Pharma Sc*. 2000; 21:35-37

Xu W, Orr-Urtreger A, Nigro F, Gelber S, Ballard Sutcliffe C, Armstrong D, Patrick J, Role LW, Beaudet AL, De Biasi M. Multiorgan autonomic dysfunction in mice lacking the β2 and β4 subunits of neuronal nicotinic acetylcholine receptors. *J Neurosc.* 1999; in press

Zoli M, Le Novere N, Hill Jr. JA, Changeux J-P. Developmental regulation of nicotinic ACh receptor subunit mRNAs in the rat central and peripheral nervous system. *J Neurosc.* 1995; 15(3): 1912-1939

The Effect of Fat Content and Degree of Fat Emulsification on the Structure-Functional Relationship of Cheddar Cheese

GUINEE, T.P., AUTY, M.A.E., MULLINS, C., CORCORAN, M.O. AND MULHOLLAND, E.O.

Dairy Products Research Centre, Teagasc, Moorepark, Fermoy, Co. Cork, Ireland

Reduction in fat content and delivery of desirable heat-induced functionality are considered two of the major approaches by which international cheese consumption can be increased. Yet, little has been reported on the effect of fat reduction or the degree of fat emulsification on the functionality of cheese. The objective of the current study was to examine the effect of fat content and degree of fat emulsification on the heat-induced changes in microstructure, viscoselasticity and functionality of Cheddar-style cheeses.

The following cheeses were manufactured at pilot plant level in 500-l cheese vats: full fat cheese (FFC; 30% w/w fat), full fat cheese from homogenised milk (FFCH; 31.6 % w/w fat), half-fat cheese (HFC; 17.4% w/w fat) and low fat cheese (LFC; 1.3% w/w fat). The cheeses were ripened at 7 °C for 180 d. The intact casein level was calculated from contents of total protein and pH 4.6 insoluble N. The microstructures were examined before and after heating to 90 °C using confocal laser scanning microscopy. Dynamic changes in viscoelasticity on heating, from 20 to 82 °C, were measured using low amplitude strain oscillation rheometry on a controlled stress rheometer. The stretch was measured by uniaxial extension of the molten cheese at a velocity of 0.066 ms^{-1} following heating in an electric-fan oven at 280 °C for 4 min. Flow was defined as the % increases in diameter of a cheese disc on heating at 280 °C for 4 min.

Reduction in fat level resulted in increases in the contents of cheese moisture and intact casein, and in the density of the *para*-casein matrix. Fat in the unheated FFC and HFC cheeses occurred as discrete globules and larger irregular-shaped fat areas occluded within the *para*-casein network; the degree of clumping of fat globules increased as the concentration of fat increased. In contrast to the FFC, fat in the FFCH occurred as an emulsion of smaller discrete, rounded fat droplets of uniform size. Heating of the FFC and HFC cheeses to 90 °C resulted in coalescence of fat globules, an effect that increased with increasing fat content. The fat globules in the FFCH were very thermostable and did not clump or coalesce on heating. Heating resulted in a decrease in the elastic shear modulus (G') and increase in the phase angle (δ) in all cheeses. In the FFC and HFC, δ increased slowly from ~12- 15° to ~ 25 -30 ° as the temperature was raised from 20 °C to ~ 45°C and thereafter more rapidly reaching values of ~ 50-70 ° at 82 °C. In contrast, the FFCH and LFC cheese samples did not exhibit the abrupt increase in δ at temperatures > 45 °C and attained values for δ at 82 °C that were much lower than those of the FFC and HFC. Reduction in fat content and increasing the degree of fat emulsification, by homogenization of the cheesemilk, resulted in reductions in δ_{max}, the magnitude of which decreased in the following order: FFC (~ 65–70°) > HFC (~40–55 °) > LFC (~ 40–50 °) > FFCH (~ 30–40°). The flow and stretch of the melted cheese were markedly impaired by homogenization of the cheesemilk and by lowering the fat content, especially to levels <17.4% w/w. The stretch and flow of values for the LFC and FFCH were similar and markedly lower than those of the FFC and HFC.

Fat content and degree of fat emulsification have a marked effect on the microstructure and heat-induced flow behaviour and functionality of cheese. It is hypothesised that fat liquefaction and coalescence contribute to the increase in fluidity of the melting cheese, as reflected by the large increase in δ at temperatures > 45°C. Fat coalescence also results in free oil which, when exuded at the surface of the melting cheese, lowers the degree of moisture evaporation, thereby enhancing its flow and stretch.

Kelvin Force Microscopy Used to Study Electronic Properties of Materials

M.E. HAWLEY

Los Alamos National Laboratory, Los Alamos, NM, USA

A combination of new scanning probe techniques has been developed over the last few years to meet the need for understanding the relationship between microstructure and extrinsic properties. These combinations are used in a two-pass mode of operation to obtain the structural detail with the corresponding map of the property of interest. An example of one such successful technique is used in the magnetic force microscope, which takes advantage of the fact that magnetic interactions are long-range. A line-by-line measurement is made in tapping mode first on the surface, then at a fixed height above the surface, outside the range of Van der Waals interactions, to obtain magnetic information from the stray field emanating from the surface. The same is true for Kelvin force microscopy, which also employs a combination of alternating contact and noncontact scans to simultaneously obtain topography and contact potential variation maps. Kelvin force has been used to reveal a variety of new electronic information such as variations of work function on surfaces and discontinuities at grain boundaries.

Multi-photon spectroscopy of plant tissues

FU-JEN KAO, PING-CHIN CHENG*, CHI-KUANG SUN†, BAI-LING LIN‡, YI-MIN WANG, JIAN-CHENG CHEN, YUNG-SHENG WANG, TZU-MING LIU† AND MAO-KUO HUANG

Department of Physics, National Sun Yat-sen University, Kaohsiung, Taiwan, ROC; *Department of Electrical Engineering, University at Buffalo, NY, USA; †Department of Electrical Engineering, National Taiwan University, Taipei, Taiwan, ROC; ‡Institute of Molecular Biology, Academia Sinica, Taipei, Taiwan, ROC

Considering its non-linear nature, two-photon excitation may generate very different spectral response in samples when compared with single-photon excitation. It is thus necessary to measure the two-photon spectra of samples, so that the fluorescence images can be properly interpreted[1]. However, fluorescence spectra obtained from bulk samples may not provide adequate information for microscopy. For instance, due to the relatively small contribution to the total fluorescence intensity, a small number of fluorescent particles in a generally fluorescing specimen may escape detection when the spectrum of the specimen as a whole is obtained. In addition, signals resulted from second harmonic generation (SHG) may be mixed with low-level broadband background auto-fluorescence commonly

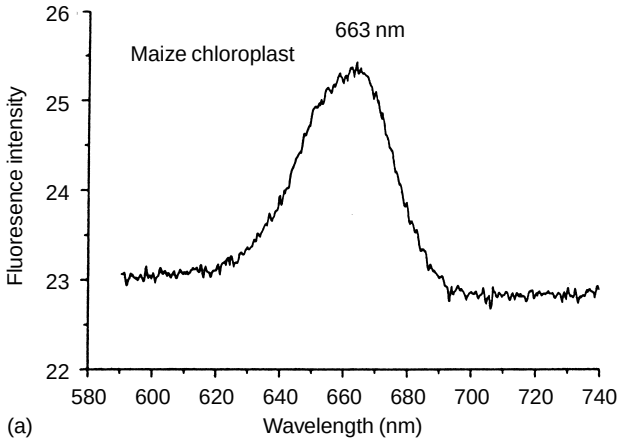

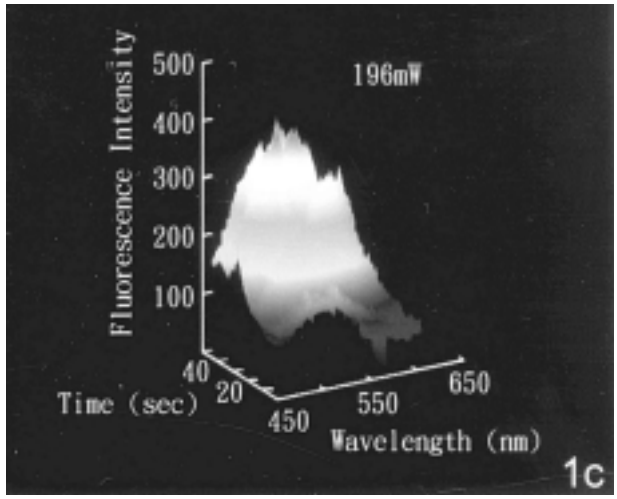

FIG.1 (a and b) Two-photon excited fluorescence of a single chloroplast in maize. (c) Three-dimensional plot of fluorescence emission spectra vs. time showing the changes in spectrum and intensity of the green fluorescence from a chloroplast under intense NIR(Ex=780nm) illumination.

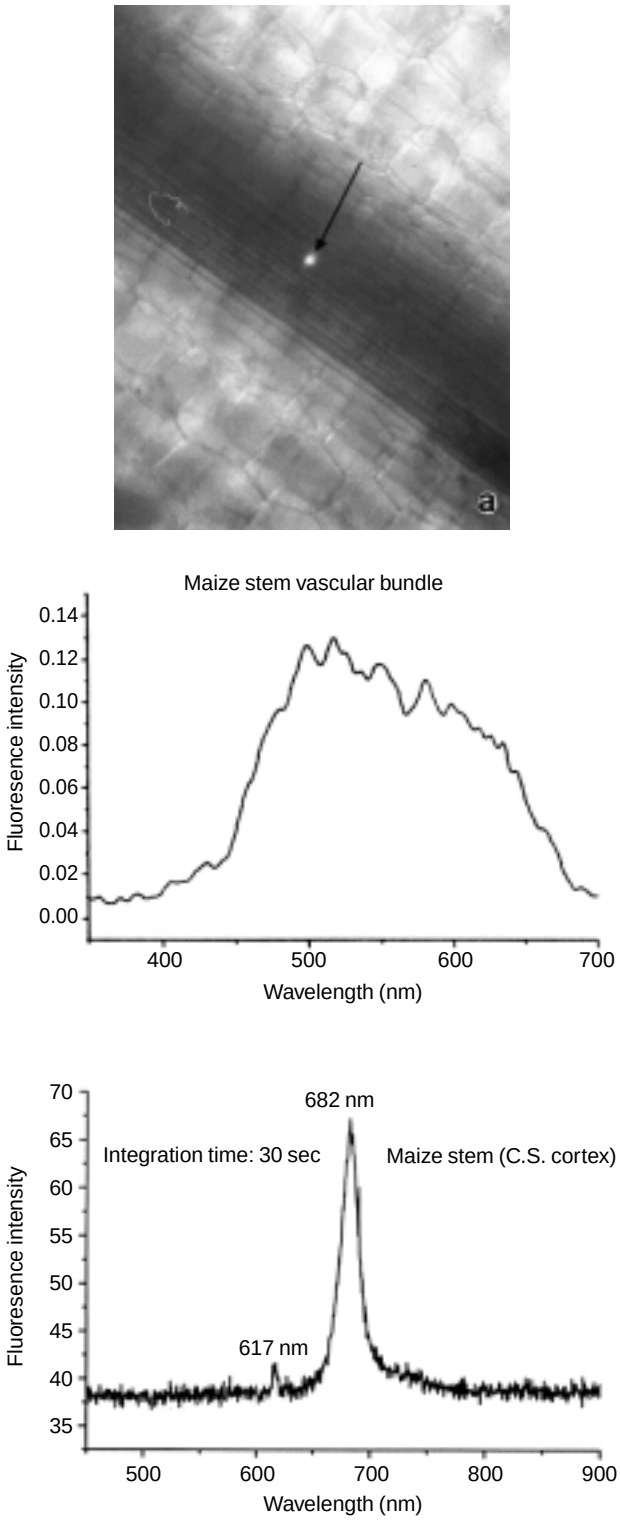

FIG.2 (a) Transmission micrograph of a longitudinal section of maize stem. Arrow in the center of the micrograph indicates two-photon excited fluorescence emission generated by a tightly focused IR beam. (b) The fluorescence spectrum obtained from the spot shown in (a). (c) Spectrum obtained from the cortex in maize stem (cross-section) excited by 1234nm IR. Note the red fluorescence at 682nm and SHG at 617nm.

found in biological specimen. Therefore, measuring fluorescence spectrum from a micro-focused volume is essential to properly interpret multi-photon fluorescence images. In this study, leaf protoplasts and stem slices of maize were used as samples to address this issue in a micro-spectroscopic set-up.

Leaf protoplasts of *Zea mays* L. (Ohio43) were isolated and suspended in culture medium according to the methods of Huang and Chen[2]. Unstained stem slices of maize were also used. Two-photon induced fluorescence spectra were measured with a SpectraPro-500 spectrometer equipped with a TE-cooled PMT. The excitation laser beam (780nm, NIR) is derived from a mode-locked Ti-sapphire laser operating at a repetition rate of 82MHz with a pulse width approximately 100fs. A dichroic beam-splitter (ChromaTech-650DCSP) was used to achieve epi-illumination and on-axis fluorescence detection in a modified Olympus BX microscope. Two IR cut-off filters (Edmond Scientific, K53-710) were installed in front of the entrance slit of the monochromator to reject scattered IR from the sample. Excitation intensity of 10^{12}W/cm^2 was reached at the focal point. A second set-up using a Chromium-doped Forsterite laser, operated at 120MHz and 130fs pulse, was used for 1234nm infrared excitation.

Figure 1 shows two-photon excited fluorescence spectra obtained from a chloroplast. A prominent red fluorescence peak with emission maximum at 663nm was observed (Fig. 1a). A broadband green fluorescence emission, peaked at 532nm/550nm, was measured (Fig. 1b). The 663nm emission is the result of chlorophyll fluorescence while the origin of the 532/550nm emission is yet to be determined. Fig. 1c is a three-dimensional plot of spectra against time showing the spectral and intensity changes of the green auto-fluorescence of a chloroplast under intense NIR illumination. The technique allows detailed study of cellular damages in multi-photon microscopy. Fig. 2a is a transmission micrograph of a maize stem. Two-photon excited yellow-green fluorescence generated by a focused IR beam is clearly visible in the center of the micrograph (arrow). The fluorescence spectrum obtained from the spot is illustrated in Fig. 2b. When excited with 1234nm IR, a spectrum with red fluorescence peaked at 682nm was obtained from the cortex of maize stem. A small peak at 617nm was also observed which is likely a result of SHG in the plant cell wall (Fig. 2c).

Supported by Academia Sinica, National Science Council (NSC-89-2112-M-110-016, NSC89-2216-E-110-003,NSC-89-2215-E-002-004,NSC-88-2811-B-001-0023,NSC-89-2311-B-001-032), Ministry of Education (89-B-FA08-1-4) of ROC, and Mr. and Mrs Jin-Mu Huang of Aurum Belle Investment Co. FJK, PCC, CKS and BLL contribute equally, therefore should be considered as co-principal authors.

References

Cheng PC, Pan SJ, Shih A, Kim KS, Liou WS and Park MS: Highly efficient upconverters for multiphoton fluorescence microscopy.

J.Microscopy 189:199-212,1997.
Huang HC. and Chen CC: Genome multiplication in cultured protoplasts of two *Nicotiana* species. *J.Heredity* 79:28-32,1988.

Effects of Milk Proteins on Frozen Dough Microstructure Visualised with CSLM

SHEILA KENNY, MARK AUTY*, ELKE ARENDT

Food Science and Technology Department, University College, Cork, Ireland; *Dairy Products Research Centre, Teagasc Moorepark, Fermoy, County Cork, Ireland

The gluten network is the main structural component in yeasted dough and is responsible for gas retention. A major problem encountered with frozen dough is dough weakening which involves disruption of the gluten network by ice recrystallisation and reducing compounds from dead yeast cells. This results in excessively long proof times, low bread volume, and poor texture. Additives, especially dough strengtheners, which interact with the gluten network, are used in frozen dough to counteract weakening. Dairy proteins are added to bread for their nutritional and functional properties. Incorporation of dairy ingredients into frozen dough which improve baking quality would be beneficial compared to use of synthetic additives because of their high nutritional value and natural origin. Sodium caseinate (SC), untreated whey protein concentrate (WPC), and heat-treated whey protein concentrate (WPCHT) were incorporated into frozen dough. Baking properties were measured over a 15-week frozen storage period. Confocal scanning laser microscopy was used to view frozen dough microstructure after 10 weeks of frozen storage. Nile blue was used to visualise protein and starch. SC had a positive influence on frozen dough baking properties. It decreased proof time, increased bread volume and reduced crumb firmness. CSLM images showed that SC appears to interact with the gluten network to produce an enhanced, more continuous gluten network compared to the control. WPC increased proof time, decreased volume and increased crumb firmness. CSLM images showed that the gluten network of frozen dough with WPC appeared to be fragmented and less continuous than the control, suggesting that WPC interferes with the gluten network. Heat treatment of WPC improved its baking properties, and frozen dough with WPCHT had shorter proof time and produced bread with higher volume and lower crumb firmness compared to frozen dough with WPC. CSLM images showed that heat treatment eliminated the negative effects of WPC on the gluten network.

The Effect of pH on Heat Denaturation and Gel Forming Properties of Glycinin

CATRIONA LAKEMOND*, HARMEN DE JONGH*, TON VAN VLIET*, MARCEL PAQUES*†, HARRY GRUPPEN

Centre for Protein Technology TNO-Wageningen University, Wageningen, The Netherlands; *Wageningen Centre for Food Sciences, Ede, The Netherlands; †Unilever Research Vlaardingen, Vlaardingen, The Netherlands

Soy glycinin is the major protein in soybean, representing ca. 30% of total protein. Glycinin consists of an acidic and a basic polypeptide, linked by a single disulphide bridge, with molecular weights of ca. 38 kDa and 20 kDa, respectively. In this research we studied heat denaturation, gelation behaviour and the resulting gel structure of soy glycinin at pH 7.6 and pH 3.8 at an ionic strength of 0.5.

Glycinin was isolated from Williams'82 soybeans according to Thanh and Shibasaki (1976) by isoelectric precipitation at pH 6.4. Heat denaturation was determined by differential scanning calorimetry (DSC). Gel formation of 10% glycinin was followed by dynamic measurements in a Bohlin reometer (strain 0.01, freq. 0.1 Hz). After heating from 20-95°C at 1°C/min the samples were held at 95°C for 30 min (glycinin), and subsequently cooled down to 20 °C at 1°C/min.

"Non-network protein was defined as the protein in the supernatant obtained by centrifugation of the gel. In order to obtain the "network" protein slices of 40 (m were cut from a gel. Next, the soluble fraction was allowed to diffuse out of the slices during 24 hours by adding excess buffer. From the protein concentration of the non-network protein fraction the total proportion of non-network protein was calculated. The composition of the protein (ratio acidic versus basic polypeptides) was obtained by SDS PAGE followed by densitometric analysis. CSLM pictures were obtained with a LEICA TCS SP microscope with a 63(objective. A data restoration procedure was performed afterwards to remove blur and noise in order to recover relevant detailed information that is present but concealed in the unprocessed data.

References

Thanh, V.H. and Shibasaki, K., (1976), J. Agric. Food Chem., 24, 1117-1121.

The Response of Maize Protoplasts in Multi-photon Fluorescence Microscopy

BAI-LING LIN, FU-JEN KAO*, PING-CHIN CHENG†, RANG-WU CHEN, MAO-KUO HUANG*, YUNG-SHENG WANG*, JIAN-CHENG CHEN*, YI-MIN WANG*, WAYNE Y. CHENG‡

Institute of Molecular Biology, Academia Sinica, Taipei, Taiwan, ROC; *Department of Physics, National Sun Yat-sen University, Kaohsiung, Taiwan, ROC; †Department of Electrical Engineering, University at Buffalo, NY, USA; ‡Williamsville East HS, Williamsville, NY, USA

Considering the low linear absorption coefficient in the near infrared (NIR) range, multi-photon fluorescence microscopy has been cited for its advantage in increased depth penetration in biological specimen[1]. Currently, mode-locked Ti-sapphire and Cr-Forsterite lasers that generate sub-picosecond pulses are employed as light sources for multi-photon fluorescence microscopy. However, it is conceivable that at high illumination intensity, non-linear photochemical processes may generate adverse effects on cell physiology and viability in ways much different from low illumination in the linear domain. Therefore, the relationship between cell damage and peak power has become an interesting and much debated topic[3].

Leaf protoplasts of *Zea mays* (Ohio43) were isolated from seedlings at 4th leaf emerging. The protoplast culture consists of a mixture of mesophyll, epidermal and bundle sheath cells. To evaluate cell survival under high intensity illumination, protoplasts were loaded with 2μM of Calcein AM for 15min prior to examination. Two-photon fluorescence microscopy was performed on a modified Olympus Fluoview confocal microscope equipped with a mode-locked Ti-sapphire laser operated at 780nm (100fs pulse, 82MHz). An Olympus water immersion objective (UPLANApo60xW-PSF, NA=1.2) was used in this experiment. A 650nm short-pass dichroic beam splitter (ChromaTechnology-650DCSP) was used to guide the illumination beam. The average and peak power densities at the focal point approximate $3x10^6 W/cm^2$ and $3.9x10^{11} W/cm^2$, respectively. We have also constructed a two-photon micro-spectroscopic setup to measure the time-dependent fluorescence decay in a chloroplast[2]. The peak power at focal point is approx. $3.7x10^{10} W/cm^2$.

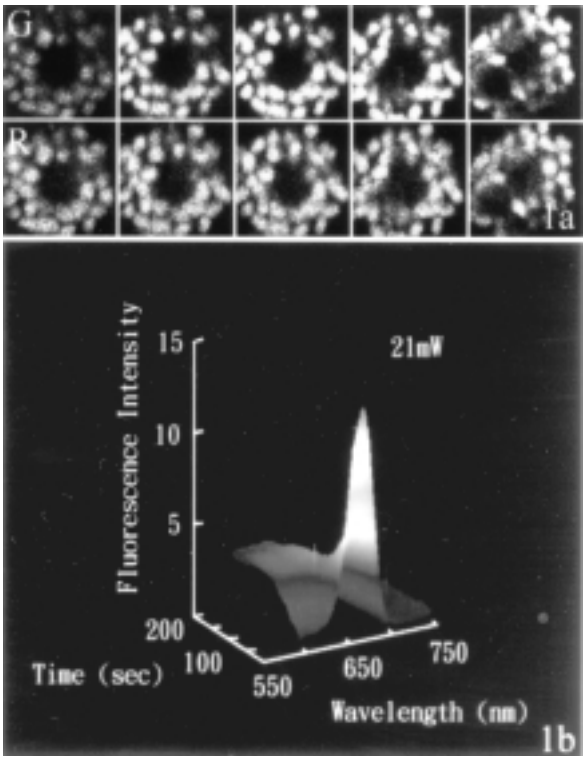

FIG. 1 (a) Time sequence of NIR exposure (left to right) to a maize mesophyll protoplast. Note the rapid increase in fluorescence intensity initially in both the green (G) and red (R) fluorescence series. The average energy exerted on the specimen for each pixel is approximately 54nJ for each scan. (b) Micro-spectroscopy of a single chloroplast showing the rapid decay of red fluorescence.

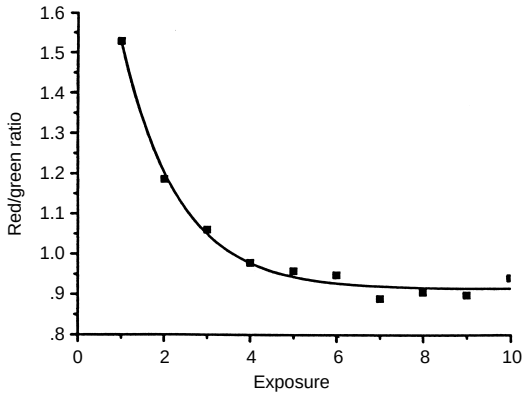

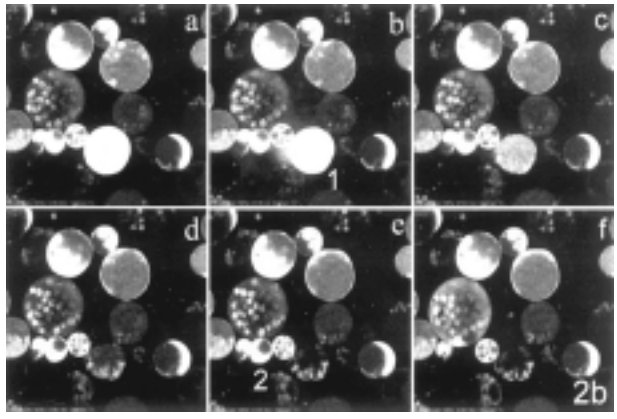

FIG. 2 (a) Fluorescence intensity ratio (red/green) plotted against NIR exposure showing an exponential decay function. The total energy exerted on each pixel is 54nJ x number of exposures. (b) Green fluorescence images of a time sequence of NIR exposure to Calcein AM loaded maize protoplasts. (a) represent the first exposure with the dose indicated in Fig. 1b, (b): 5th, (c): 10th, (d) 15th, (e): 20th and (f): 25th exposure. Note cell #1 in (b) expelled Calcein during the 10th scan, and cell #2 in (e) burst during the 25th scan.

Maize protoplasts exhibit a strong red fluorescence peaked at 663nm and a broadband greenish fluorescence peaked at 570nm (Fig. 1a). The 663nm emission is the result of chlorophyll fluorescence while the origin of the 570nm emission is as yet unidentified. Upon high intensity NIR irradiation, maize protoplasts show an initial increase, followed by a rapid decrease in both green and red autofluorescence. Fig. 1b shows a rapid decay of red fluorescence as a function of increasing NIR exposure. The red fluorescence intensity has a higher rate of decay, resulting in a green-shift of the fluorescence image. An image showing a similar green-shift phenomenon in a different species, *Arabidopsis thaliana*, is shown in the cover photo of this issue. When the ratio of red and green fluorescence intensity is plotted against NIR exposure, an exponential decaying function is evident (Fig. 2a). Using Calcein dye-retention as a live-cell indicator, cell survival can be identified by measuring the red/green fluorescence ratio. Fig. 2b shows a sequence of NIR irradiation to maize protoplasts loaded with Calcein AM. These results and the recently characterized linear absorption and multi-photon fluorescence properties indicate that maize protoplast can be used as a model system in the study of cell responses to high intensity illumination.

Supported by Academia Sinica, National Science Council (NSC-89-2311-B-001-032, NSC-89-2112-M-110-016, NSC-88-2811-B-001-0023), Ministry of Education (89-B-FA08-1-4) of ROC and Mr. and Mrs. Jin-Mu Huang of Aurum Belle Investment Co. BLL, FJK and PCC contribute equally, therefore should be considered as co-principal authors.

References

1. Cheng PC, Lin BL, Kao FJ, Gu M, Xu MG., Gan XS, Huang MK and Wang YS: Multi-photon fluorescence microscopy –the response of plant cells to high intensity illumination, *Micron*, in press,2000
2. Kao FJ, Lin BL and Cheng PC: Multi-photon fluorescence micro-spectroscopy, *SPIE Proceedings*, 3919, in press, 2000
3. Konig K, So PTC, Mantulin WW and Gratton E: Cellular response to near-infrared femtosecond laser in two-photon microscopes. *Optics Lett*. 22:135-136,1997

Combining Model Directed Image Analysis with Feature Directed Model Refinement in Detecting Line Segments on Confocal Microscopy Images

JAGATH SAMARABANDU, CHANDIMA EDIRISINGHE*, PING-CHIN CHENG†

Dept. of Electrical and Computer Engineering, University of Western Ontario, Canada, *Life Imaging Systems, London, Ontario, Canada †University at Buffalo, Amherst, USA

In this paper, we present an image analysis system for images obtained from a confocal laser scanning microscope (CLSM) with particular emphasis on segmentation techniques for extracting linear structures. Confocal microscopy provides the ability to capture 3D images of microscopic structures. Typical examples of the applications of confocal microscopy are demonstrated in the on-going studies of investigation of cell organization in the apical meristem of maize (Bommineni and Cheng, 1990) and the study of DNA replication sites in the nuclei of mouse 3T3 fibroblasts by BrdU labeling technique (Meng *et al.*, 1991, Samarabandu *et al*., 1992).

Image analysis methods can be categorized as data-driven or model-driven approaches. In a data-driven or bottom-up method, image data is used to detect image primitives such as edges, which are then used to instantiate a model. In a model-driven or top-down approach, a model is instantiated first using domain knowledge and used to extract image primitives that correspond to the instantiated model. Combining these methods yields a powerful image analysis system where one approach is used to feed back information to the other approach (Kanade, 1980). With the increased availability of low-cost powerful computer systems, such complex analysis systems have adequate performance to be practical. In this application, we are interested in automatically detecting and measuring line segments in semiconductor circuits. The images are processed with a combination of noise suppression using median filters and edge detection (Canny, 1986). This results in a binary image with thin contour segments that indicate each detected edge. 2D connected component labeling was then used to identify each individual contour segment. A local curvature measure coupled with an appropriate threshold is then used to detect line segments. These line segments are then merged based on gradient, intercept and endpoint proximity to form longer lines. Generation of these line segments completes the model directed phase of the analysis system. In the model refinement phase, these line segments are then classified according to its gradient and intercept. This allows grouping of line segments with different thickness. Within each group, lines are then paired based on the average image intensity in the area between adjacent line segments. These strips now form a refined model, which depicts the conductor segments, and are used to analyze the physical characteristics of these segments. This system has shown to be accurate and fairly robust in early implementations. An attractive feature is its ability to use a small number of strong image features to establish early hypotheses and then refine these hypotheses using a large number of weak image features. We are currently working on a framework that allows this system to be adapted to a wide variety of models.

References

1. V. R. Bommineni and P. C. Cheng, The use of confocal microscopy to study the developmental morphology of shoot apical meristems: A procedure to prepare the specimens, Maize Genetics Cooperative Newsletter, 64:34, 1990
2. J. F. Canny, A computational approach to edge detection, IEEE

PAMI, 8(6):679-698, 1986
3. T. Kanade, Region Segmentation: Signal vs. semantics, Computer Graphics and Image Processing, 13:279-297, 1980
4. C. Meng, J. Samarabandu, R. Acharya, T. H. Lin, P. C. Cheng and R. Berezney, The study of DNA replication sites in mammalian cell by confocal light microscopy and multi-dimensional image analysis, Scanning, 13:117-117, 1991
5. J. Samarabandu, R. Acharya, P. C. Cheng, Aspects of confocal image analysis, Biomedical Image Processing and Three-Dimensional Microscopy, Proc. SPIE 1660: 791-797, 1992

Scanning Electron Microscope Studies of Dietary Fiber of Cereals (Rice, Wheat, Jowar), Pulses (Greengram, Blackgram, Redgram and Bengalgram) and Spice (Fenugreek)

L.SINGOTAMU* AND P.RAMULU**

*Ultrastructure Unit, Pathology Division, **Analytical Food Chemistry Division, National Institute of Nutrition, Indian Council of Medical Research, Hyderabad, India

Fiber is found to be an important component of diet. Dietary fiber consists of a heterogeneous mixture of macromolecules with varying degrees of cross-linking to form a complex matrix. The major cell wall components are cellulose, hemicellulose, lignin, amyloids, pectin substances, beta-glucans and glycoproteins. Dietary fiber comes from the cell wall of food grains or seeds, fruits and vegetables in which nutrients are stored in a highly protective manner. The majority of the people in Western developed countries eat highly refined foods which contain less fiber and are associated with diseases such as diabetes, atherosclerosis, cardiovascular syndromes, colon cancer, large bowel disorders, obesity, etc., whereas in underdeveloped and developing countries such as Africa and India, respectively, people consume whole grain foods which contain high dietary fiber content and they do not suffer from the abovementioned ailments as in the West. Multiple mechanisms seem to play a role in producing a wide spectrum of effects associated with the intake of dietary fiber, such as anti-atherosclerotic and anti-carcinogenic co-relations which are found in epidemiological studies include bile salt binding, water holding capacity, alterations in alimentary transit time, modification of gut flora and interference with the trace element absorption. Fiber may also interact directly with the mucosal cell to produce a fundamental change in the intrinsic absorptive capacity of the intestinal tract. Chronic intake of dietary fiber bring changes in the ultratopography of the intestinal tract. Hence we studied the ultrastructure of insoluble and soluble dietary fiber by scanning electron microscope. We used the dietary fiber of rice, wheat, fenugreek, jowar blackgram, bengalgram and redgram after separating the soluble and insoluble fractions of dietary fiber by the AOAC method. The material was a dried vacuum desiccator at low atmospheric pressure 2 x 10^{-2}. Samples were placed on SEM stubs with double adhesive tape coated with gold by a Hitachi High Vacuum Evaporator HUS-56B. Samples were scanned by a Hitachi SEM-S520 operated at 10-15KV, and pictures were taken at appropriate magnification.

The three-dimensional arrangement of cellulose favours the formation of strong intermolecular and intramolecular hydrogen bonding. The cellulose is present in the form of microfibrils, consisting of several molecular chains, which make up macrofibrils. Arrangement of microfibrils to form macrofibrils is explained by transmission electron microscope studies in polysaccharide gels used in foods. The fiber in cooked and uncooked common bean (*Phaseolus vulgaris*) is studied by a scanning electron microscope. In the present study, we scanned the insoluble and soluble fractions of dietary fiber of rice, wheat, jowar, fenugreek, blackgram, greengram, redgram and bengalgram. Scanning electron microscope studies revealed that the ultratrophotographic structure of soluble dietary fiber (cereals and pulses) has loosely assembled microfibrils. Hence it has more water holding capacity by formation of cross-links due to intra- and inter-molecular hydrogen bond formation. Insoluble dietary fiber has tightly twisted or compactly arranged microfibrils. It has less water holding capacity. In general, dietary fiber forms a mesh which has bile salts adsorbing property. Microflora also gets trapped in it. Fermentation and gas formation take place in the intestine. Dietary fiber has a role to play in the hard to cook aspect of pulses. Probably the proportion or percentage of dietary fiber present in the grains and seeds has a role to play in the cooking aspects of cereals and pulses. Fenugreek dietary fiber has a role to play in the prevention and control of diabetes.

Scanning Electron Microscope Studies on Malaria Specific Immune Response of Lymphocytes in Malarial Patients

L. SINGOTAMU, S. A. KUMARI

Ultrastructure Unit, Pathology Division, National Institute of Nutrition, Hyderabad, India

Malarial infection leads to release of endotoxin; i.e., hemin due to the constant burst of RBC during schizogany, which induces macrophages to release a range of mediators. Hemin, being in free-radical form, is pyrogenic in nature. Due to its chemotactic effects, a series of pathological responses occur, which mainly include fever and activation of the hypothalamo-pituitary-adrenal axis. Due to the pyrogenic action of hemin, the immune CNS system gets communicated and activation of an arachidonic acid cascade; i.e., prostaglandins, takes place. This stimulates the HLA gene to produce specific m-RNA, which, in the cytoplasm, synthesizes specific cytokines which trigger differentiation of malarial fever specific lymphocytes from the bone marrow stem cells. In the paper we are reporting ultrastructural morphology of lymphocytes in malaria com-

pared with lymphocytes of influenza and typhoid patients.

Blood samples of 4 ml each were collected in heparinised vials from malaria patients of the National Malaria Eradication Programme, influenza and typhoid patients from Sir Ronald Ross Institute of Tropical and Communicable Diseases, Hyderabad, India. To every sample, 6 ml of 0.2M PBS was added and mixed well. From this 4 ml was added to the 3 ml of ficol hypaque from the side of the culture tube. These samples were centrifuged at 2500 RPM for 30 minutes at room temperature. Lymphocytes were collected from the ring, which is formed between the blood saline mixture and ficol-hypaque. These lymphocytes were washed with 0.1M PBS and centrifuged at 2000 RPM for 10-15 minutes. 0.87% ammonium chloride was added to the pellet to lyse the left over RBC and washed again with 0.1M PBS. Pelleted samples were fixed in 1% buffered glutaraldehyde for one hour at 4°C. Samples were centrifuged and washed with PBS and distilled water. Thus formed pellets of cells were suspended in 0.5 ml of distilled water. These cells were placed on pre-cooled (methanol bath -70°C) SEM stubs and dried in RFS freeze dryer (model 3110 BLT) for 2 hours. These samples were coated with gold (300 A) in an HUS 5GB vacuum evaporator and scanned under a Hitachi (S520) scanning electron microscope, operated at 10-15 K.V. Required pictures were taken at appropriate magnifications and prints were made accordingly.

In control lymphocytes are found in clusters with blunt pseudopodia which may help in phagocytosis. In acute malarial infection, different kinds of lymphocytes are found. One type of lymphocyte is spherical with blunt digitations on the surface. Another kind has fenestra. Surfaces of these lymphocytes have micro bulbous punctate digitations and tail-like extensions. In cases of acute malaria, it is found that infected RBC are encountered by two types of lymphocytes. It appears as a cytotoxic phenomena. In cases of moderate malarial infection, parasitized RBC appear to be studded with immunoglobulin complex like bodies. Their surfaces, which may damage the parasitized RBC, act as mitogen. We scanned lymphocytes of viral fever (influenza) and bacterial fever (typhoid) patients for comparison and found lymphocytes of different ultrastructural morphology in each case. Differences in the ultrastructural morphology of lymphocytes suggests that the infection-specific lymphocytes are stimulated or activated by specific cytokine mediators while differentiating and releasing the lymphocytes from pluripotent bone marrow stem cells.

Quenching of Energy of Cancerous Cells by using Antioxidants — A Scanning Electron Microscope Study

L.SINGOTAMU AND K. KRISHNASWAMY

Ultrastructure Unit, Pathology Division, National Institute of Nutrition, Indian Council of Medical Research, Hyderabad, India

Cancerous cells irrespective of organ and tissue will have a set of common properties, such as cell to cell contact. Inhibition process is lost and they appear similar to a grape bunch. Cells become porous in the cell cycle, and the S phase is prolonged. Growth rate of cells will be high but cell age decreases and death rate is high (apoptosis) when compared to normal cells. Cytoplasm becomes gel, and cytoskeleton gets distorted. The integrated dynamic spatial network is found to be largest in neoplastic cell and pH of the cell gets altered, biochemical and physiological process of the cell starts operating at higher amplitude of energy dynamics. Ultrastructure of surface topography of some of these properties of dysplastic cells and oral cancerous cells were observed by scanning electron microscopy.

Thin and uniform human cervical smears were prepared on glass slides from Ayer's spatula scrapings. These smears were fixed in 1% buffered glutaraldehyde for 3 hrs. Smears were washed in distilled water to remove excess fixative. In order to avoid staining and mounting damage to the cells, a layer of glycerine was spread over the smears (to maintain the refractive index of cover glass). In these smears, normal, mild, moderate severe dysplastic cells were identified and marked with a diamond scoring pencil, based on cytoplasmic and nuclear ratio by light microscope. Glycerine is washed out by distilled water. Oral biopsy samples were collected from MNJ Cancer Hospital, Hyderabad, India, and washed with washing solution (1% sodium carbonate in 0.1 M. PBS with pH 8) in order to remove mucus debris. Samples were fixed for 1 hr at 4°C in buffered 70% ethanol, saturated with mercuric chloride and sucrose was added to maintain the osmolality and tonicity of the tissue. After washing in distilled water both cervical and oral samples were dehydrated by ethanol grades and acetone (intermediate fluid). Samples were covered with amylacetate (transitional fluid) and dried in a chemical vacuum desiccator. Samples were coated with gold and palladium (300-350A) and scanned under a Philips SEM 510 operated at 7 to 15 KV. Pictures of interesting areas were taken at appropriate magnifications in 120 mm Indu film and SEM pictures of required size were printed.

The process of energy dissipation of the cell distils from the glycolysis and tricarboxilic acid cycle to facilitate in manifestation of energy. The imbalance in the endogenous and exogenous generation of energy coupling dynamics leads to cancerous growth of cells. It might be due to free radical generation. The accumulation of free radicals creates an environment for operation of non-newtonian

mechanics to operate at a molecular level due to the difference in the density of electrons by free radicals, irrespective of size of molecules. Thus cells may develop into cancerous cells. To curb this abnormal proliferation due to free radical production, one has to use foods containing antioxidants, i.e., chromophores (vitamin bearing colour photo sensitizing pigments) of either plants or animals, such as carotenoids, xanthenoids (green or yellow leafy vegetables/fruits) and sterols such as calciferol and *tocopherol*, etc., whose bond energy should be within a range of minimum 200 nm to maximum 700 nm of wavelength of electromagnetic continuum which will act synergistically in quenching amplitude of energy of cancerous cells, in order to revive from cancerous to normal cells. Photodynamic therapy states that pigments (photosensitizer pigments; i.e., hematoporphyrin derivatives, act as antioxidants) in combination with light or laser beam used as therapeutic agents of cancer.

Scanning Electron Microscopy EDX-ray Analysis of Millets (finger millets, foxtail millets and pearl millets)

L. SINGOTAMU

Ultrastructure Unit, Pathology Division, National Institute of Nutrition, Indian Council of Medical Research, Hyderabad, India

Millets are the crop of the common masses, as they form the staple diet of the common people. As the bulk of the produce is consumed at the village or rural level, the real value of millets as a crop group has not been appreciated, and their importance is not recognized in imparting food security to a large section of the farming community. Small millets include finger millets, foxtail millets, pearl millets, kodo millets, little millets, barnyard millets, and proso millets. These crops are becoming less popular because our staple food range is now limited to high yielding hybrid crops of wheat, rice, etc., so nutrient resources are delimited. In general, these crops are pest-resistant, and cultivable in dry land. A wide spectrum of nutrients such as proteins, carbohydrates, minerals and dietary fiber are available in these millets. These crops are cost-effective because a high quantity of manure is not needed for their yield. Disorders such as diabetes, obesity, etc., could be prevented or controlled by consumption of these grains. Millets are grown in about 20 million hectares world-wide and the major growing countries, apart from India, are China, Russia, Japan and certain African and European countries. Millets form an excellent bird feed in which China is a major player. There is also demand for processed and value-added products of these millets. In countries such as Japan, a big movement on local food traditions is taking shape, wherein the emphasis is on coarse grains. However, not much work has gone into the diversification and value addition for these cereals. There is a need to encourage the traditional food habits. The main reason hindering the mass consumption of these cereals is the lack of awareness. In the present study, we scanned pearl millets, finger millets and foxtail millets by scanning electron microscope in order to know about their ultrastructural characteristics as well as the elemental composition pattern by the EDX method of SEM.

Ten grams of each sample of finger millet, pearl millet and foxtail millet were collected from the genebank curator of ICRISAT, Hyderabad, India. These samples were cut transversely and longitudinally by a razor blade and mounted on SEM stubs with double-sided adhesive tape. They were coated with gold 300A° thick in a HUS-5GB vacuum evaporator and scanned by the Hitachi S-520 SEM operated at 10-15 KV. Required pictures were taken using 35 mm film at appropriate magnification and negatives were developed and prints made. The same samples were ground, powdered and placed on an SEM stub with double-sided adhesive tape, coated with gold and analysed in a Link ISIS-300 Oxford model of EDX-ray accessory attached to a Hitachi S-520 SEM in order to know the elemental composition pattern of these millets. Data and graphs were printed by laser printer.

In Indian pearl millet, *pennisetum glaucum*, cells are compactly filled with carbohydrate granules which are paracrystalline in pattern. McDonough and Ronney studied the American pearl millet *pennisetum americanum* by scanning electron microscopy, the carbohydrate granules being in globular form. Elemental analysis was done by SEM EDX-ray, which revealed that the oxygen is 47.77%, carbon is 45.88%, iron is 2.83%, potassium is 2.35%, silicon is 0.63%, magnesium is 0.54% in composition pattern of these elements. By SEM and fluorescence microscopy, McDonough, Ronney and Earp studied the ultrastructure of *Eleusine corocana* finger millet. Our SEM studies revealed that the nutrient granules are pleomorphic in nature. SEM EDX-ray elemental analysis recorded 48.04% of carbon, 42.03% of oxygen, 4.54% of copper, 2.45% of calcium, 2.18% of iron, 0.76% of silica in composition pattern of elements. We studied the ultrastructural characteristics of foxtail millet *Setaria italica*. In T.S. cells appear in a honeycomb pattern and small spherical starch granules are embedded in them. SEM-EDX-analysis revealed that oxygen is 53.69%, carbon is 44.59%, iron is 1.18%, potassium is 0.40%, silica is 0.14% in the composition pattern of elements. Calcium and copper are recorded only in finger millet. Magnesium is present only in pearl millet. Potassium is present in pearl millet and foxtail millet. Carbon, oxygen, iron, and silica are present in all three. Intake of a millet diet may be omitted, restricted or recommended in the practice of Indian medicine (Ayurveda), since it has a significant role to play in the patients with diabetes, obesity, etc. Moreover, the millet diet is economical. This kind of study enhances the awareness of the nutritional potential of millets to become popular for routine consumption.

Scanning Electron Microscope Studies on Role of Silicon in Skeletal and Dental Fluorosis in Experimental Rats

L. SINGOTAMU

Ultrastructure Unit, Pathology Division, National Institute of Nutrition, Indian Council of Medical Research, Hyderabad, India

Around the globe, 23 nations including India are affected with fluorosis due to consumption of fluoride contaminated water. Reports say that intake of an optimum dose (or lower limit) has no effect on human health[3] and intake of a high dose of fluoride has effects on skeleton called "skeletal fluorosis"[1] and on teeth called "dental fluorosis"[2]. The soft tissues such as gastrointestinal tract also get affected by fluoride intake[4,5]. The present study is aimed at understanding the interaction of silicon with fluoride. Its impact on bone mineralization, enamel and dentine formation is studied by the scanning electron microscope. 48 male weanling litter mate rats (NIN Wistar strain inbred-A line) of similar body weights were equally (12 each) divided into the following 4 groups : 1 - experimental control with normal silica and normal fluoride diet. 2 - high fluoride (HF-150 ppm). 3 - high silicate (HSi-1000 ppm) and 4 - high fluoride-high silicate diet (HF + HSi). The basic diet contains 20% casein, 80% starch and 5% groundnut oil with complete vitamins and minerals. After 9 months of experiment, rats were sacrificed, lower and upper incisors and femur were dissected out and cleaned with distilled water and washing solution (1% $NaHCo_3$ in normal saline), and dehydrated in ascending series of acetone, and air dried. Incisors and femur bone were fractured by a cutting player so that the internal surface was exposed to the electron beam. These samples were coated with gold and palladium in a polaron sputter coating unit and scanned by a Philips scanning electron microscope operated at 10-15 KV. Pictures were taken at appropriate magnification by a 36 mm camera and prints were made at required size. Food intake, growth rate and body weights of all groups of rats were similar. Administration of fluoride alone, in combination with silicate, produced typical fluorotic changes in the incisor teeth of all rats. These changes are more significant or prominent in the rats fed with high fluoride and high silicate. In control rats, fractured incisors showed a typical pattern of crystallites in the enamel region and dentine is highly compact. Femur bone endosteal and cut surfaces showed a normal pattern of ossification in HF fed rats. Enamel does not show an orderly pattern of crystallites and dentine is not compact with blood vessel passages. Femur endosteal surface is not calcified. There is no mineral deposition on collagen bundles; here and there bone resorption areas are seen. In the high silicate fed group, arrangement of crystallites of enamel is not in order. Dentine looks like a lumpy mass. Endosteal surface of femur shows blood vessel passages, which are obliterated. However, collagen bundles are not mineralised. In the high silicate and high fluoride fed group, crystallites of enamel are large. Dentine is compact and shows blood vessel passages. In the endosteal surface of femur, ossification is not perfect. Passages for blood vessels are completely obliterated. It is observed that in high silicate and high fluoride fed rats, incisors grow out of the oral cavity. This tendency reminds one of the elephant's ivory tusks which are formed in the place of premolars. Weight of femur bone increased as compared to control.

References

1. Susheela AK, Arbind Kumar, Madhu Bhatnagar and Rashmi Bahadur. *Prevalence of endemic fluorosis with gastrointestinal manifestations in people living in some north Indian villages.* Fluoride 26, 2, 97-104 (1993).
2. Susheela AK, Madhu Bhatnagar, Gnanasundram N. and Saraswathy T.R. *Structural aberrations in fluorosed human teeth. Biochemical and scanning electron microscopic studies*. Current Science 77, 12, 1677-1681 (1999).
3. Susheela AK. *Fluorosis management programme in India* Current Science 77, 10, 1250-1256 (1999).
4. Das TK, Susheela AK, Gupta IP, Dasarathy S. and Tandon RK. *Toxic effects of chronic fluoride ingestion on the upper gastrointestinal tract.* J. Clin. Gastroenterol. 18, 194-199 (1994).
5. Dasarathy S, Das Taposh K, Gupta IP, Susheela AK and Tandon RK. *Gastroduodenal manifestations in patients with skeletal fluorosis.* J. Gastroenterol. 31, 333-337 (1996).

Scanning Electron Microscope (SEM) Studies on Milk Samples of Buffalo, Goat, Cow, Sheep, Ass, Human and Commercial Dairy Milk Samples

L. SINGOTAMU

Ultrastructure Unit, Pathology Division, National Institute of Nutrition, Jamai Osmania Hyderabad, India

SEM is a useful instrument for studying the microstructure of a variety of food materials and many food properties have been shown to be related to the structures found by microscope. Chemical and physical analysis of raw materials and intermediate and commercial finished products are important to the dairy industry. From the microscope point of view, milk consists of constituents which are corpuscular and have dimensions such as fat globules, casein micelles, submicellar casein making them visible. In the present study we are reporting the ultrastructural analysis of milk samples in order to know the nutrient composition pattern. Buffalo, cow, sheep, goat, ass, human and two commercial dairy milk samples were collected and freeze dried in a lypholizer. Samples were placed on SEM stubs with double adhesive tape and coated (300Å) with gold in a Hitachi High Vacuum Evaporator HUS-5GB. These samples were scanned by a Hitachi SEM operated at 10-15 KV and pictures were taken at appropriate magnification. Sheep, goat, human and ass milk contain very

low percentages of fat and proteins (casein, lactalbumin and lactoglobulin) as compared to buffalo and cow, but they contain a higher percentage of sugar or lactose in non-crystalline form as compared to buffalo and cow. There is a very high content of fat with large fat bodies in the milk of buffalo, as compared to cow milk, so the ghee of buffalo is kept in preference to the cow. In the cow milk, proteids are less as compared to buffalo milk. A striking ultrastructural feature of crystalline of flakes is observed in ass milk, which may be of lanceolate calcium phosphate. Thus sheep, goat, human and ass are having almost similar ultrastructural nutrient composition pattern. But it appears to differ in proportion. Buffalo and cow have common ultrastructural nutrient composition patterns but it appears to be differ in their proportion of nutrients. In India, ass milk is used as an indigenous home therapeutic agent for neonates since it has a high percentage of heat generating calcium phosphate; i.e., lactose and calcium phosphate. The cow milk has characteristic "phospholipids", proteins which are found in the grey matter of the brain, so it is popularly known to brighten the intellect. Goat milk is known for its medicinal significance probably owing to its higher digestibility, its alkaline reaction and its higher suitability to weak stomachs, since fat globules of goat are smaller than those of cow and buffalo. Ultrastructural features of sheep milk are more or less similar to goat milk. Human milk appears to be more comprehensive in its nutrient composition (i.e., fat globules, lactose, proteins, vitamins and minerals) pattern when compared to sheep, and goat which may be ideal to feed infants. In two commercial dairy milk samples, one has casein. In another sample, moderate fat bodies are found. These milk samples are commercially processed and stored and suppliable to the public as samples in which different components are extracted and supposed to be left with the desired quantity of milk components; i.e., fat bodies, casein, etc. This milk is meant for routine domestic use. Thus SEM is found to be a technologically viable tool for understanding the ultrastructure of natural as well as commercial milk samples.

The Automated-EBSP System in the Materials Characterization Lab

JOHN A. SUTLIFF

HKL Technology, Burnt Hills, NY, USA

The automated electron backscattering pattern (EBSP) technique for electron diffraction in the scanning electron microscope (SEM) can be used efficiently to perform some important microstructural analyses. This paper gives an introduction to some of the common analyses requested at a modern EBSP facility. In each case, the attributes of modern automated-EBSP analysis are used to advantage: the ability to analyze polished sections without the need for etching; the use of both stage and beam automation to efficiently collect data from multiple samples and sample locations; the high angular accuracy and quantitative nature of the crystallographic analysis, and, finally, the high rate of data acquisition.

Of all analyses requested, grain size determination was the most common in the author's laboratory. Determining grain size with good reproducibility and repeatability in materials having grain size of ASTM #12 to #16 can be difficult and time-consuming using conventional optical or SEM systems with image analysis. This is typically so because the samples must be etched. Fine-grained samples, especially multiphase samples, can give confusing and/or inconsistent images in the etched condition. Using an automated-EBSP system, diffraction patterns are collected at small intervals (0.05 to 2 microns) along test lines through the un-etched microstructure[1]. These patterns are analyzed and the intercept lengths across the sampled grains are measured based on the calculated lattice misorientation between points. When the microstructures examined have a high density of twins or are heavily deformed, conventional microscopy is even more difficult and the advantage of the EBSP technique, where the quantitative analysis of misorientation across boundaries is sustained, is even greater. Using stage automation, grain size can be measured for three to six samples in one SEM session with multiple locations analyzed. A single grain size determination having high statistical quality can be made in about half an hour.

The second most numerous request in the author's lab was for microtexture analysis. The materials scientist uses this type of analysis to assess the degree of microstructural non-uniformity in crystallographic texture that results from the fabrication or subsequent processing of a specimen. The spatial variations in texture are determined from the diffraction patterns collected throughout the microstructure with particular attention to sampling an adequate number of grains over meaningful surface areas in the material's volume. Examples might include: assessing the change in alignment (texture gradient) from surface to mid-plane in a rolled aluminum plate; assessing the size of alpha colonies in a hot worked titanium alloy; and determining the rate at which texture components develop in a CVD coating. If line scans are utilized, such as for grain-size analysis, one can efficiently study any relationship between texture components and the grain size distribution as a function of macro-location in the specimen[2].

An analysis using automated-EBSP that is becoming more common is the measurement of plastic deformation. When materials are deformed they can store much of the plastic strain energy in sub-grain structures that generate local lattice rotation[3]. Automated-EBSP is able to quantify the amount of sub-grain lattice rotation and in combination with calibration data can be used to accurately relate the microstructure of an unknown to that of microstructures with known plastic strain[4,5]. A recent application of this kind of analysis was the evaluation of retained plastic strain in the heat-affected zone (HAZ) of stainless steel

welds[6]. Analysis of the sharpness of features in EBSP can also yield information on plastic strain[7].

Many additional types of analyses are requested in the EBSP facility and it is of primary importance to realize that the automated-EBSP technique is a general crystallographic technique. It is a good replacement for any kind of micro-Laue experiment particularly if the samples are very small and hard to handle (such as fine fibers) or if they are multiphase and tend to produce rather confusing patterns or if you are looking for a very minor constituent. With the beneficial flexibility of SEM sample manipulation, automated-EBSP is quick and efficient as a "point-and-shoot" crystallographic analysis and phase identification tool[8]. Sometimes the question is as simple as, "Is this feature in my microstructure crystalline?" and EBSP provides a quick and cheap technique to get the answer.

Like other even more mature microanalysis techniques, automated-EBSP analysis must be carefully performed or artifacts and erroneous data may be obtained. Also, EBSP analysis is a surface technique (~ top 100 nm) and therefore analysts must take care to understand the surface condition of their specimens and the role of surface preparation in the analysis. With reasonable care, the automated-EBSP technique provides materials characterization professionals with a productive tool for obtaining very useful quantitative microstructural data.

References

1. J. A. Sutliff, "Grain Size Analysis Using Automated-EBSP", Microscopy and Microanalysis 5 (Supp. 2: Proceedings) (1999) 248-249
2. S. Vogel *et al.*, "Effect of texture on the development of grain size distribution during normal grain growth" Scripta Materilia 34 (1996) 1225
3. H. Weiland, "In-Situ Observation of Deformation Processes by OIM" Microscopy and Microanalysis 3 (Supp. 2: Proceedings) (1997) 567-568
4. D. Juul Jensen, "Grain Subdivision During Deformation Studied by Automatic EBSP" Microscopy and Microanalysis 5 (Supp. 2: Proceedings) (1999) 232-233
5. J. A. Sutliff, "An Investigation of Plastic Strain in Copper by Automated-EBSP" Microscopy and Microanalysis 5 (Supp. 2: Proceedings) (1999) 236-237
6. Angeliu *et al.*, "Intergranular Stress Corrosion Cracking of Unsensitized Stainless Steel in BWR Environments" Presented at 9th Environmental Degradation Conference, August 1999, Newport Beach, CA. in press
7. A. Day and G. Shafirstein, "Assessment of local residual strain by electron backscatter patterns and nanoindentation" Materials Science and Technology 12 (1996) 873-879
8. J.A. Small and J. R. Michael, "Phase Identification of Individual Particles by Electron Backscatter Diffraction (EBSD)" Microscopy and Microanalysis 5 (Supp. 2: Proceedings) (1999) 226-227